Radiolysis-Assisted Direct Growth of Gold-Based Electrocatalysts for Glycerol Oxidation

Nazym Tuleushova, Aisara Amanova, Ibrahim Abdellah, Mireille Benoit, Hynd Remita, David Cornu, Yaovi Holade, Sophie Tingry

Highly-Dispersed Ni-Pt Bimetallic Cocatalyst: Synergetic Effect Yields Pt-Like Activity in Photocatalytic Hydrogen Evolution

Cong Wang,[a] Diana Dragoe,[b] Christophe Colbeau-Justin,[a] Paul Haghi-Ashtiani,[c] Mohamed Nawfal Ghazzal,[a] Hynd Remita[a,*]

a. Institut de Chimie Physique, UMR 8000 CNRS, Université Paris-Saclay, 91405 Orsay, France.
b. Institut de Chimie Moléculaire et des Matériaux d'Orsay, UMR 8182 CNRS, Université Paris-Saclay, 91405 Orsay, France.
c. Laboratoire de Mécanique des Sols, Structures et Matériaux, CNRS UMR 8579, CentraleSupélec, Université Paris-Saclay, Gif-sur-Yvette, France.
Corresponding Author: hynd.remita@u-psud.fr

ABSTRACT

Achieving high photocatalytic activity with the lowest possible platinum (Pt) consumption is crucial for reducing the cost of Pt-based cocatalysts and enabling large-scale applications. Bimetallic Ni-Pt cocatalysts exhibit excellent photocatalytic performance and are considered as one of the most promising photocatalysts capable of replacing pure Pt for the hydrogen evolution reaction (HER). However, the synergistic photocatalytic mechanism between bimetallic Ni-Pt cocatalysts needs to be further investigated. Herein, we deposit highly dispersed Ni-Pt bimetallic cocatalysts on the surface of TiO_2 by radiolytic reduction. We study the dynamics of photogenerated charge carriers of the Ni-Pt co-modified TiO_2 and propose their underlying electron transfer mechanisms, in which Pt acts as an electron trap, whereas Ni serves as an electron supplier. The synergistic effect is Ni/Pt ratio-dependant, and can confer bimetallic Ni-Pt to pure Pt-like photocatalytic activity in HER. The Ni_2-Pt_1 co-modified TiO_2 is optimized to be the most cost-effective photocatalyst with robust stability, which outperforms about 40-fold higher performance than bare TiO_2.

KEYWORDS: bimetallic cocatalysts, synergetic effect, dynamics of photogenerated electrons, photocatalytic hydrogen evolution, solar fuels.

1. INTRODUCTION

Solar-to-hydrogen conversion via photocatalysis promises a bright future in simultaneously addressing global environmental issues and energy shortages.[1-3] Titanium dioxide (TiO_2) is the most popular photocatalyst due to its excellent chemical stability, high resistance to photocorrosion, and low toxicity;[4] However, limited solar light absorption and rapid photogenerated charge recombination restrict its widespread practical applications.[5-7] To overcome these obstacles, loading with metal cocatalysts is a facile and effective approach to improve the photoactivity of TiO_2.[8] These metal cocatalysts, especially noble metal cocatalysts, not only can reduce the energy barrier of proton reduction, but also can serve as electron traps to promote the photogenerated charge separation by virtue of their lower Fermi levels.[9] Platinum (Pt) is considered as the most efficient cocatalyst ascribable to its higher work function, extremely low required overpotential and optimal hydrogen adsorption free energy.[10-12] Nevertheless, the commercial application of Pt in large-scale is greatly hampered by scarce reserves, high price, and susceptible corrosion.[13] Reducing the dosage of Pt without sacrificing its performance is an issue that needs to be solved imminently in the photocatalytic energy conversion.

Alloying or association of Pt with inexpensive and abundant transition metals (TMs, e.g., Ni,[14] Fe,[15, 16] Co,[17] and Cu[18]) has been gradually recognized as a feasible route to diminish Pt consumption. Bimetallations between Pt and TMs allow the formation of unique electronic properties and extraordinary synergistic effects, offering great potential for achieving enhanced photocatalytic performance.[19, 20] Benefiting from the Pt-like work function and relatively high H atom adsorption energy, Ni is possibly the most logical and promising alternative TM to Pt.[21] The Ni-Pt bimetallic cocatalyst enables to effectively improve the sluggish kinetics of photocatalytic hydrogen evolution reaction (HER).[22] Substantial effort has been devoted to the morphology design, size customization, and compositional allocation of Ni-Pt bimetallic cocatalysts.[23-25] However, the underlying synergistic mechanism between Ni-Pt remains ambiguous in spite of the excellent photocatalytic efficiency.

The dispersion of the cocatalyst is another factor affecting the photocatalytic performance.[26] High dispersibility cannot only reduce the usage of cocatalyst, but also favor suppressing the agglomeration and growth of cocatalysts during the HER.[27] In light of that, we employed the powerful radiolytic reduction technology to synthesize highly dispersed Ni-Pt co-modified TiO_2 photocatalysts in this work.[28, 29] In comparison with pure Pt-modified TiO_2, the partial substitution of Ni could lead to synergistic effects, enabling bimetallic Ni-Pt to Pt-like activity in photocatalytic HER. The degree of synergy could be tuned by varying the ratio of Ni/Pt, where Pt serves as an electron trap and Ni acts as an electron supplier. The density and lifetime of photogenerated charge carriers of mono- or co-modified TiO_2, which are key factors in photocatalysis, were tracked via a time-resolved microwave conductivity technique. The Ni_2-Pt_1 co-modified TiO_2 was found to be the most cost-effective photocatalyst with robust stability.

2. EXPERIMENTAL SECTION

Chemicals and materials. Titania (TiO_2-P25, 80% anatase and 20% rutile, Evonic), nickel (II) acetylacetonate [$Ni(acac)_2$] (≥95%, Sigma-Aldrich), platinum (II) acetylacetonate [$Pt(acac)_2$] (≥99.98%, Sigma-Aldrich), triethanolamine (≥99%, Sigma-Aldrich), and ethanol (≥99.9%, Sigma-Aldrich) were used without further purification.

Synthesis of the photocatalysts. Ni-Pt/TiO_2 photocatalysts were synthesized by radiolytic reduction of Ni^{II} and Pt^{II} complexes. Radiolysis is a powerful method to synthesize metal nanoparticles of controlled size, shape and structure in solutions, heterogeneous media or on supports. The reducing species (solvated electrons and alcohol radicals) are produced in situ from the interactions between the ionizing radiation and the solvent. They induce a homogeneous reduction and nucleation leading to metal nanoparticles.[30-32] Typically, 200 mg TiO_2-P25 were dispersed in 20 mL ethanol,[33] the needed amount of the metal precursors was added to the suspension (**Table S1**). The obtained suspensions were stirred for 2 hours in order to adsorb the Ni^{II} and Pt^{II} complexes on TiO_2 surface, and then deaerated with nitrogen gas under stirring for 20 min and subsequently irradiated for 6 h for complete reduction of the metal ions with a ^{60}Co panoramic gamma source with a dose rate of 4 kGy h^{-1}. After irradiation, the samples were washed 3 times with ethanol, centrifuged, and dried in an oven at 80 °C overnight. The UV-visible spectra of the supernatant show no absorption and attest that all the metal is deposited on TiO_2. Finally, grey powders were obtained. The samples were labelled as A%Ni, A%Pt and A%Ni_x-Pt_y, where A is the total mass loading, x and y are the mass proportions of Ni and Pt.

3. RESULTS AND DISCUSSION

The Ni^{II} and Pt^{II} complexes were reduced by solvated electrons (e_s^-) and alcohol radicals induced by solvent radiolysis (**Figure 1a)**. The total mass loading of metal was 0.1% for all the photocatalysts. With changing the added contents of Ni and Pt precursors, Ni_x-Pt_y/TiO_2 photocatalysts with different Ni/Pt mass ratios, including 0.1% Ni, 0.066% Ni, 0.1% Ni_3Pt_1, 0.1% Ni_2-Pt_1, 0.1% Ni_1-Pt_1, 0.1% Ni_1-Pt_2, 0.1% Ni_1-Pt_3, 0.033% Pt and 0.1% Pt were synthesized. The morphology of Ni-Pt/TiO_2 photocatalysts is revealed by high-angle annular scanning transmission electron microscopy under bright-field and dark-field (HAADF-STEM), emphasizing highly dispersed ultrasmall Ni and Pt nanoparticles (NPs) deposited on the surface of TiO_2 (**Figure 1b-d** and **Figure S1)**. The location of the metal NPs is further identified by the energy-dispersive X-ray spectroscopy (EDS) mapping of STEM, illustrating the independent homogenous distribution of Ni and Pt over the TiO_2 surface (**Figure 1e** and **Figure S2d)**. It is worth noting that the NPs were reduced separately during the deposition process, and no nanoalloys were observed. This could be attributed to the weak metal interactions, which can be caused by the very low metal loading and/or the low interaction of the metal complex with TiO_2.

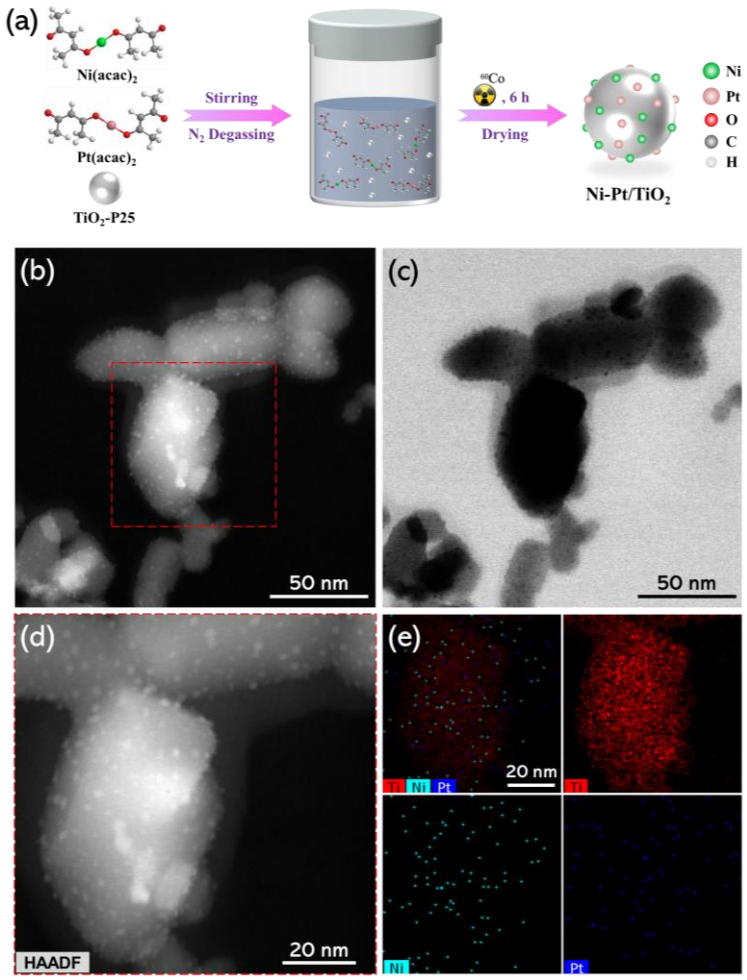

Figure 1. (a) Synthetic schematic of Ni-Pt/TiO_2 photocatalysts. HAADF-STEM images of 0.1% Ni_2-Pt_1/TiO_2 films under (b) dark-field and (c) bright-field showing the highly dispersed metal nanoparticles. (d, e) STEM-EDS elemental mapping of 0.1% Ni_2-Pt_1/TiO_2 showing independent homogenous distribution of Ni and Pt NPs.

Low- and high-resolution transmission electron microscopy (HRTEM) were employed to offer a further insight into the nanostructures of Ni-Pt/TiO_2 (**Figure 2, Figure S2a-c** and **Figure S3)**. As shown in **Figure 2a**, the average size of Ni-Pt NPs is determined as 1.9 nm, which approximately corresponds to an optimal particle size of Pt in photocatalytic applications.[34, 35] HRTEM images reveal lattice fringes of 2.28 Å and 1.9 Å, corresponding to (111) and (200) planes of Pt, indicating the formation of crystalline Pt NPs (**Figure 2c**).[14] The crystal lattices of Ni are identified as to be 2.4 Å and 2.1 Å corresponding to the NiO (111) and NiO (200), respectively (**Figure 2c**).[11] Notably, the Ni and Pt NPs are physically in contact with TiO_2 to form multi-junctions, which could offer additional pathways for the transfer of electrons, thus inducing high photocatalytic activity.[36]

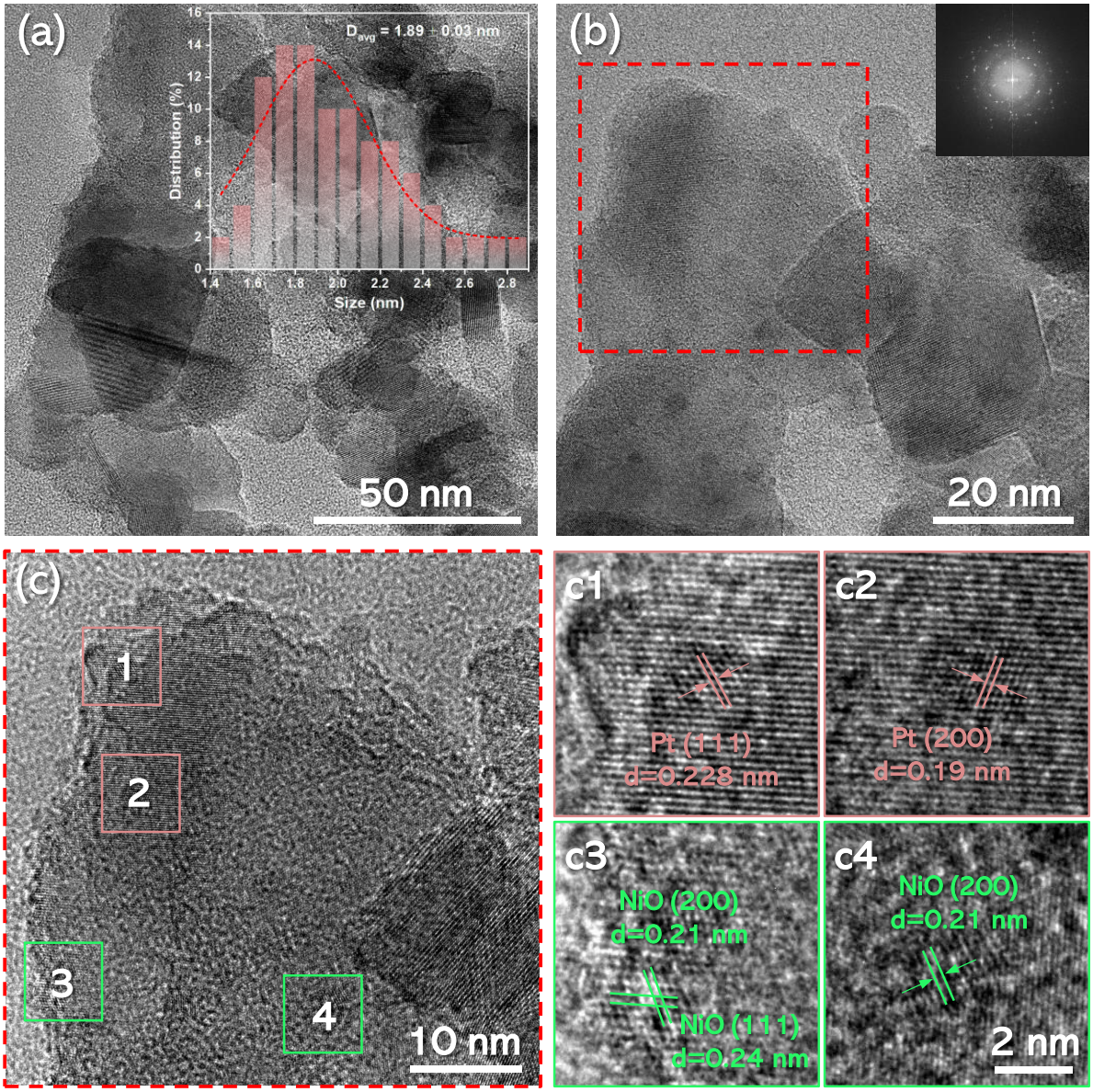

Figure 2. (a, b) TEM images of 0.1% Ni_2-Pt_1/TiO_2. The inset in panel (b) is the corresponding SADE pattern. (c) HRTEM images of 0.1% Ni_2-Pt_1/TiO_2 showing the crystal lattices of Ni and Pt.

The surface composition and the oxidation states of the Ni and Pt metal NPs in Ni-Pt/TiO_2 are analyzed by X-ray photoelectron spectroscopy (XPS). The general XPS surveys of Ni-Pt/TiO_2 only indicate the presence of Ti, C and O species, mainly due to the low metal loading (**Figure S4**). The core-level spectra of Ti 2p for Ni-Pt/TiO_2 before irradiation shows the characteristic peaks for Ti $2p_{3/2}$ and Ti $2p_{1/2}$ at 458.5 eV and 464.3 eV, respectively, corresponding to Ti^{4+} in TiO_2 (**Figure 3a**).[37] The Ni 2p XPS spectrum shows the presence of Ni metal alongside its oxide and hydroxide. Even if Ni ions were completely reduced by radiolysis, the ultrasmall Ni metal NPs are very sensitive to oxygen and are oxidized in air.[38] Therefore, the remaining small amount of Ni^0 (with its main component Ni $2p_{3/2}$ having a BE of 852.7 eV) is expected to be located between the interphase of TiO_2 and the oxide of Ni.[39, 40] **Figure 3b** shows a superposition of reference spectra corresponding to Ni^0, $Ni(OH)_2$ and NiO (obtained for pure and well-characterized polycrystalline samples) and our samples.[41] Several peaks

corresponding to Ni^0, $Ni^{\sigma+}$ ($0 < \sigma < 2$), Ni^{2+} and their satellite peak can be observed from Ni 2p XPS spectra (**Figure 3b**).[42, 43] The details concerning the fit are given in **Figure S5**. **Figure 3c** displays the superposition of Pt 4f core-level spectra which is normalized on Ti 3s.[44-46] Difference spectrum shows an increase in the metallic Pt concentration after irradiation (**Figure 3d**). The Pt 4f spin-orbit coupling doublet is clearly visible, with Pt $4f_{7/2}$ located at 71.7 eV, having a FWHM of 1.1 eV. The decomposition of Pt 4f spectra is not performed as a quantification of different types of Pt is difficult to evaluate given the low intensity of the signal. Various valence states of Pt NPs can offer higher active sites and more oxygen vacancies, which are beneficial for surface chemisorption and catalysis.[47] X-ray diffraction (XRD) measurements were performed to confirm the crystal structures of as-prepared Ni-Pt/TiO_2 photocatalysts (**Figure S6**). The XRD patterns of all samples show similar peaks to TiO_2-P25, where the peaks at 2θ = 25.3 and 27.4 are characteristic lines of anatase (A(101)) and rutile (R(110)), respectively.[48] No diffraction peaks associated to Ni and Pt species are observed due to the small size of the clusters and to the ultralow loading of Ni or Pt in TiO_2-P25 (less than 0.1%), which is below the detection capability.

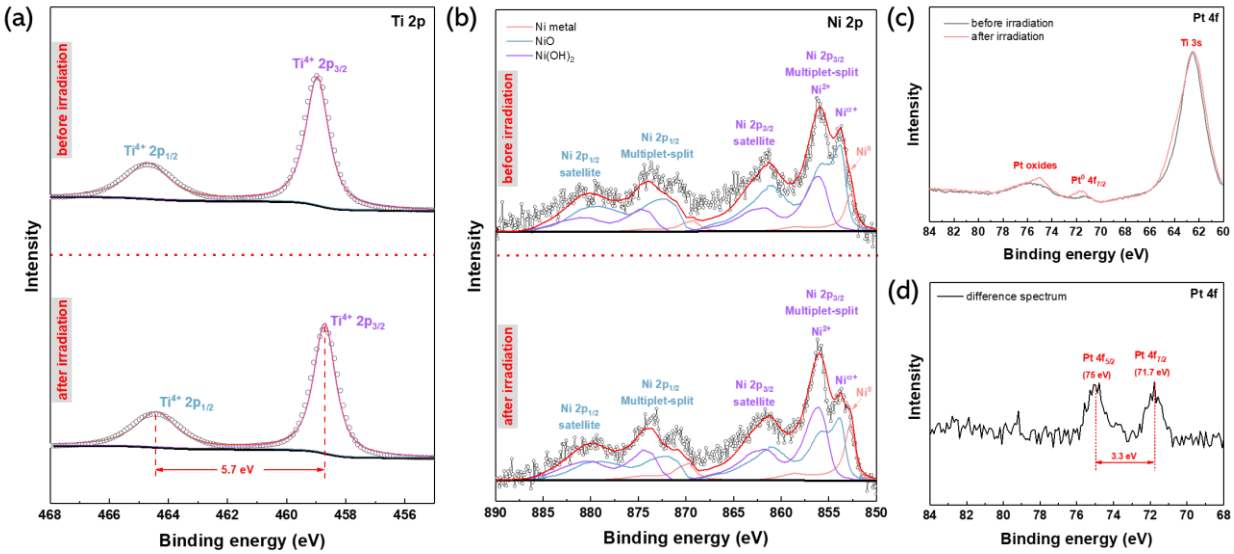

Figure 3. (a) XPS spectra of (a) Ti 2p, (b) Ni 2p and (c) Pt 4f in 0.1% Ni_2-Pt_1/TiO_2 before and after irradiation. (d) Difference spectrum of Pt 4f before and after irradiation.

The optical properties of the as-prepared Ni-Pt/TiO_2 photocatalysts are investigated by UV-vis diffuse reflectance spectra (DRS). The samples show a large absorption band in the UV region starting at 380 nm, typical of the intrinsic interband absorption of TiO_2. Noticeably, the deposition of Ni and Pt NPs redshifts the light absorption and improves its intensity in the visible region, which is slightly enhanced with the increase in Pt content (**Figure 4a**). The bandgaps of Ni-Pt/TiO_2 photocatalysts are estimated using Kubelka-Munk (K-M) theory. In agreement with the absorption, Ni-Pt/TiO_2 show a narrower bandgap (2.95 eV) than bare TiO_2-P25 (3.19 eV) attributed to the low donor level produced from Ni-Pt NPs. Indeed, the surface co-modification of titania with Ni and Pt NPs contributes to modify the electronic density of states and promotes the charge carriers' separation in TiO_2, suggesting an excellent photocatalytic performance for Ni-Pt/TiO_2.[49]

Photogenerated charge (e^-/h^+) separation of photocatalysts is widely recognized as the essential factor determining the photocatalytic performance. Electrochemical impedance spectroscopy (EIS) is used to assess the interface electric charge transfer resistances of Ni-Pt/TiO_2 photocatalysts. Significant reduction of radius is observed in metals deposited TiO_2 compared to bare TiO_2-P25, with 0.1% Pt/TiO_2 exhibiting the smallest semicircle, crediting to the large work function and high exchange current density of Pt, which leads to an oriented electron flow to the Pt through the Pt/TiO_2 interface.[10] Partial substitution of Pt by Ni increases the charge transfer resistances to some extent, where 0.1% Ni_2-Pt_1/TiO_2, 0.1% Ni_1-Pt_1/TiO_2 and 0.1% Ni_1-Pt_2/TiO_2 show quite similar Nyquist plots (**Figure S7**). As a consequence, the transient photocurrent response of Ni-Pt/TiO_2 presents the same increasing trend in photocurrent intensity, suggesting efficient charge carriers' separation under light irradiation (**Figure 4c**). The photocatalytic activity of the as-prepared samples was studied for photocatalytic HER under UV-visible light. The HER tests were performed using TEOA as a hole scavenger to evaluate the photocatalytic performance of the Ni-Pt/TiO_2 photocatalysts with different mass loadings (**Figure 4d**). The 0.1% Pt/TiO_2 shows the optimal H_2 generation rate (1.27 mmol g^{-1} h^{-1}) and AQY (78.1%), which is approximately 40 times higher than bare TiO_2-P25 (0.032 mmol g^{-1} h^{-1}, AQY = 1.97%), and consistent with the results of EIS and transient photocurrent response. It should be pointed out that the performance is not altered when replacing part of Pt by inexpensive Ni. For example, the H_2 generation rate and AQY of 0.1% Ni_2-Pt_1/TiO_2, 0.1% Ni_1-Pt_1/TiO_2 and 0.1% Ni_1-Pt_2/TiO_2 are 1.26 mmol g^{-1} h^{-1} (AQY = 77.5%), 1.27 mmol g^{-1} h^{-1} (AQY = 78.1%) and 1.23 mmol g^{-1} h^{-1} (AQY = 75.6%), respectively. Considering the cost-effectiveness into account, 0.1% Ni_2-Pt_1/TiO_2 is chosen as the target for further photocatalytic research.

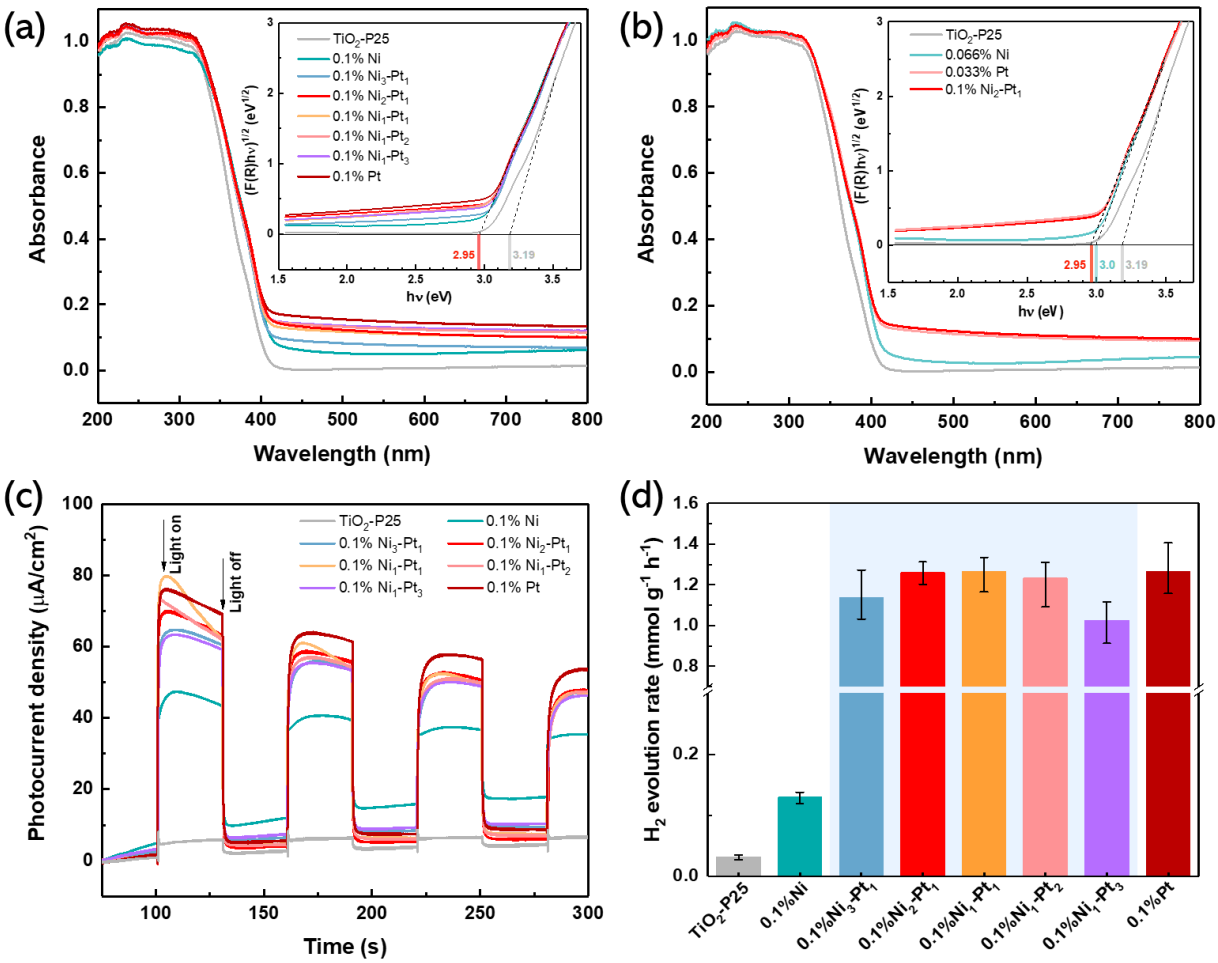

Figure 4. (a, b) UV–vis absorption spectra of TiO_2-P25, Ni/TiO_2, Pt/TiO_2 and Ni-Pt/TiO_2 with different mass loadings. The insets in panels are the corresponding Kubelka–Munk plots. (c) Transient photocurrents and (d) H_2 evolution rates of TiO_2-P25, 0.1% Ni/TiO_2, 0.1% Pt/TiO_2 and 0.1% Ni-Pt/TiO_2 with different Ni/Pt mass ratios by using TEOA as hole scavenger.

For comparison with 0.1% Ni_2-Pt_1/TiO_2, we synthesized 0.066% Ni/TiO_2 and 0.033% Pt/TiO_2 monometallic loaded photocatalysts under the same irradiation conditions. 0.033% Pt/TiO_2 shows higher light absorption compared to 0.066% Ni/TiO_2, which is close to that of 0.1% Ni_2-Pt_1/TiO_2 (**Figure 4b**). Not surprisingly, the charge transfer resistance and transient photocurrent response of 0.1% Ni_2-Pt_1/TiO_2 were found to be superior to 0.066% Ni/TiO_2 or 0.033% Pt/TiO_2, while inferior to 0.1% Pt/TiO_2 (**Figure 5a, b**). In comparison with monometallic modified TiO_2, the additional H_2 production obtained with 0.1% Ni_2-Pt_1/TiO_2 is assigned to the synergetic effect between Ni and Pt, where Ni exhibits Pt-like activities in the presence of Pt (**Figure 5c**). The wavelength-dependent H_2 evolution over 0.1% Ni_2-Pt_1/TiO_2 indicates that AQY is consistent with the UV-Vis absorption spectrum, suggesting that the H_2 evolution is dominantly driven by light (**Figure S8**). Cycling experiments were performed to attest the stability of the photocatalysts. There is no evident photocatalyst deactivation (~ 6% decrease) in the H_2 evolution measurements after five consecutive cycles, demonstrating the robust stability of 0.1% Ni_2-Pt_1/TiO_2 (**Figure 5d**). In addition, the 0.1% Ni_2-Pt_1/TiO_2 photocatalyst also shows good activities in pure water or under visible light (**Figure S9**).

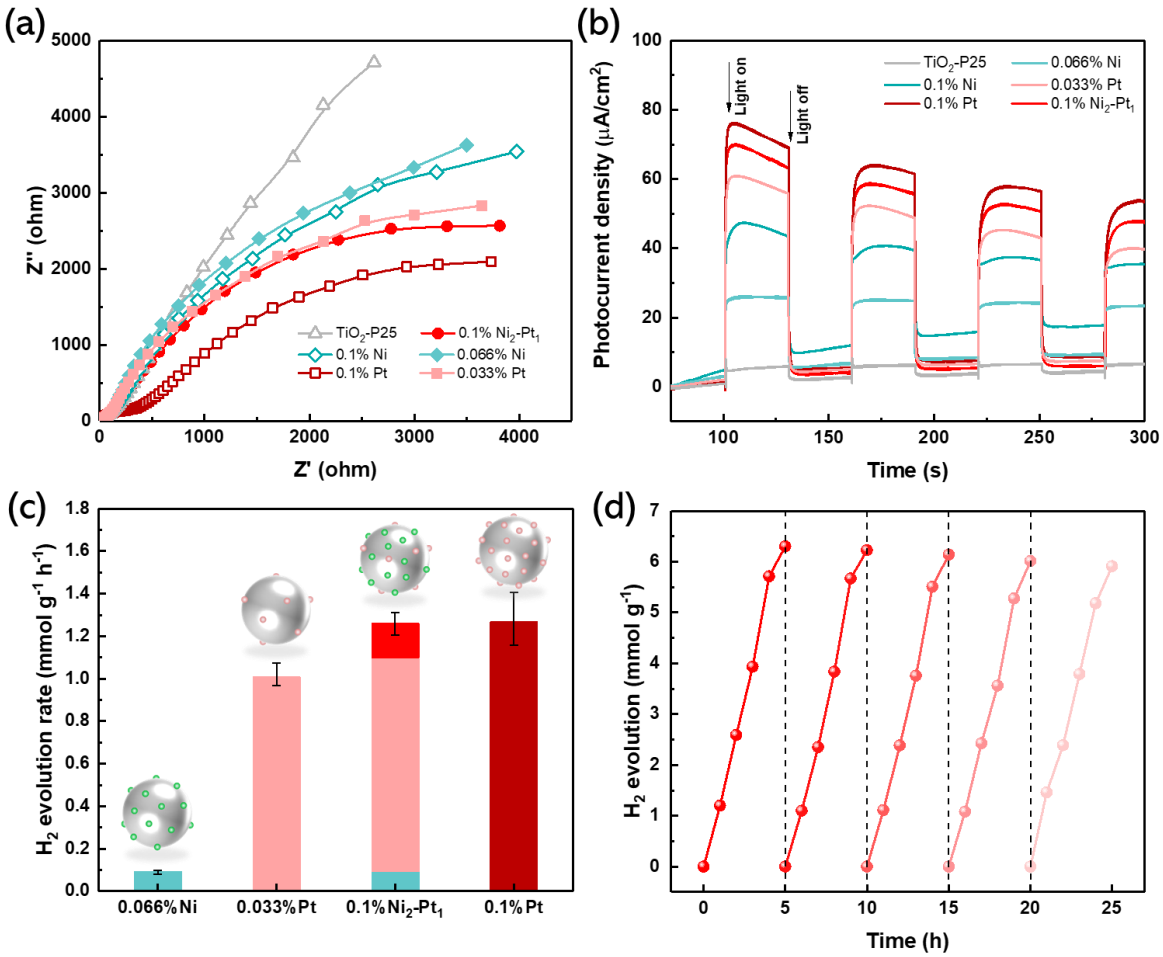

Figure 5. (a) EIS Nyquist plots, (b) transient photocurrent and (c) H_2 evolution rate obtained with TiO_2-P25, 0.066% Ni/TiO_2, 0.1% Ni/TiO_2, 0.033% Pt/TiO_2, 0.1% Pt/TiO_2 and 0.1% Ni_2-Pt_1/TiO_2. (d) Long-term HER test with 0.1% Ni_2-Pt_1/TiO_2.

To further reveal the role of Ni in the synergetic effect of Ni and Pt loaded co-modified TiO_2, TRMC measurements were performed to study the dynamics of excess electrons in the conduction band of the photocatalysts and their recombination kinetics.[50] The TRMC technique is based on the measurement of the relative change of the microwave power reflected by the photocatalyst, $\Delta P(t)$, induced by its laser pulsed illumination. The relative difference $\Delta P(t)/P$ can be correlated, for small perturbations of conductivity, with the difference of conductivity $\Delta\sigma(t)$ considering the following equation:[51]

$$\frac{\Delta P(t)}{P} = A\Delta\sigma(t) = Ae\sum_i \Delta n_i(t)\mu_i \qquad (1)$$

where A is a time-independent sensitivity factor, but depends on different factors such as the microwave frequency or the dielectric constant. The Δn_i is the density of photogenerated charge carriers "i" at known time "t", and μ_i is their mobility. Considering the small and negligible mobility of the trapped species, Δn_i is reduced to mobile electrons in the conduction band and holes in the valence band. In the case of TiO_2, the TRMC signal is mainly attributed to electrons because their mobility is much larger than that of holes.[52]

The signal obtained by this technique displays the evolution of the sample photoconductivity, $I(t)$, as a function of time (ns). The main data provided by TRMC are the maximum value of the signal (I_{max}) and the decay of the signal (the decrease of the excess electrons), which reflects the number and the lifetime of excess charge carriers created after the laser pulse excitation, respectively.[53] To analyze the decay, the signal is divided in two sections: short- and long-time decays. The short-time decay (fixed up to 40 ns after the maximum of the pulse) is represented by the I_{40}/I_{max} ratio, which reflects the fast processes mainly due to the electron-hole recombination and possibly electron scavenging by metal. A high value indicates a low recombination speed. The long-time decay (fixed from 200 to 1000 ns) is related to slow processes, which involve the interfacial charge transfer reactions and decay of excess electrons controlled by the relaxation time of trapped holes.[40] In this range, the decay of TRMC signals can be fitted to a power decay according to:

$$I = I_D \times t^{-k_D} \qquad (2)$$

where I_D is the intensity of the signal due to charge carriers that recombine after 200 ns, and K_D is an adimensional parameter related to their lifetime: higher K_D values correspond to faster decays of the TRMC signals.[54]

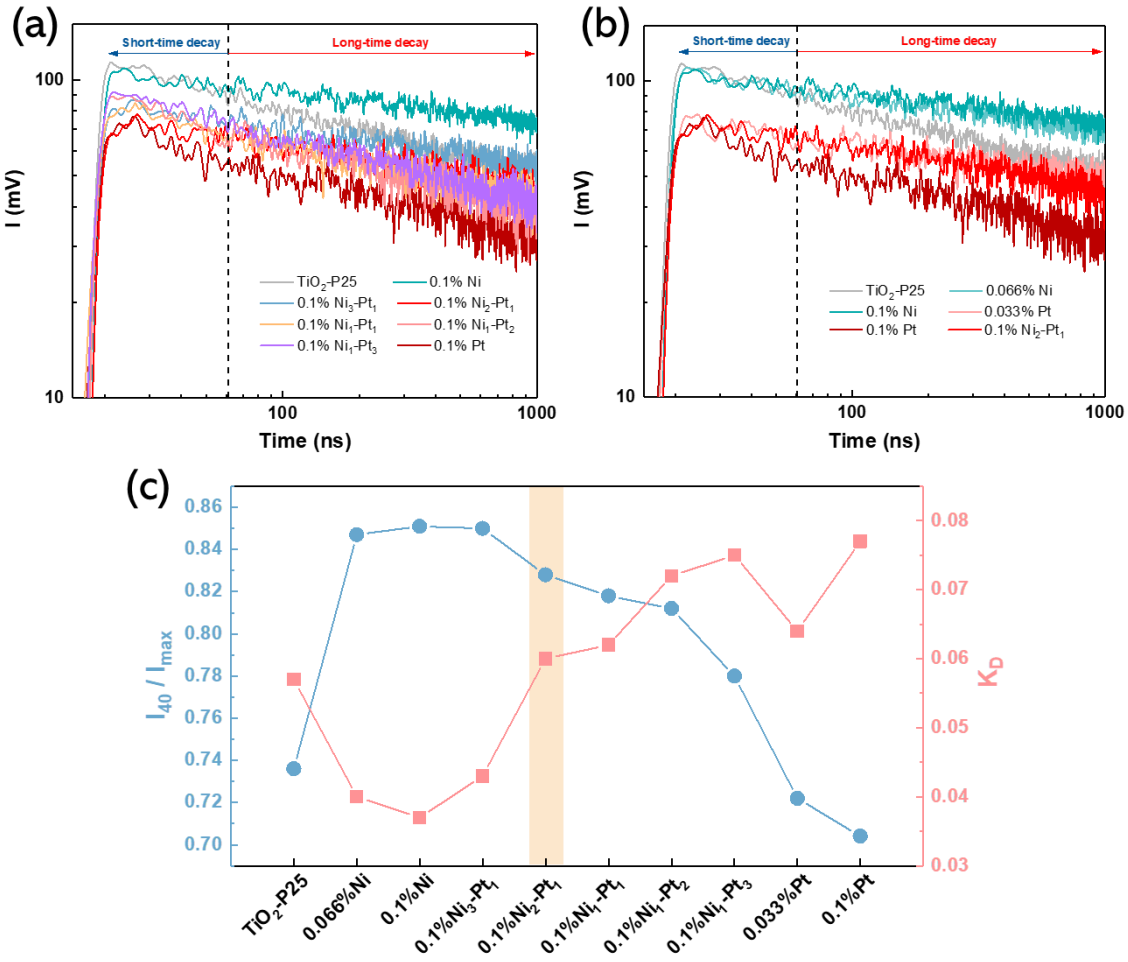

Figure 6. (a, b) TRMC signals and (c) corresponding parameters of TiO_2-P25, Ni/TiO_2, Pt/TiO_2 and Ni-Pt/TiO_2 with different mass loading.

As shown in **Figure 6a, b**, the transient photoconductivity data were displayed in double-logarithmic plots with a time scale from 10 to 1000 ns. The monometallic Pt modified or Ni and Pt co-modified TiO_2 photocatalysts show an apparent reduction in the I_{max} values compared to bare TiO_2 (**Table S2**), which can be attributed to the fast electron scavenging by the metal NPs (<10 ns).[55] In contrast, the participation of Ni alone has no significant effect on the number of photogenerated charge carriers, implying that Ni NPs may play a strikingly different role than Pt NPs in the charge carriers transfer on the metal/TiO_2 interface.[39]

As previously mentioned, the short- and long-time decays are characterized by the I_{40}/I_{max} ratio and K_D, respectively. The loading of Pt NPs leads to the decrease in I_{40}/I_{max} ratio and increase in K_D corresponding to a rapid decay of charge carries lifetime, which is mainly attributed to the excellent electron capture capability of Pt (**Figure 6c**).[31, 56] Whereas an opposite effect is observed in monometallic Ni modified TiO_2, where Ni NPs (mainly Ni_xO) appear to act as semiconductors to provide electrons rather than electron scavengers. The additional electronic donation from Ni NPs can efficiently delay the decay and extend the lifetime of charge carriers. However, it needs to be emphasized that high photocatalytic activity is not only affected by the lifetime of charge carriers, but also depends on the effective utilization of electrons. For bimetallic TiO_2 co-modified with Pt and Ni, the I_{40}/I_{max} ratio trends to decrease with increasing Pt (or reducing Ni) content, while K_D shows the opposite trend (**Figure 6c**). Among these, 0.1% Ni_2-Pt_1 and 0.1% Ni_1-Pt_1 exhibit similar charge carrier lifetimes, which are highly consistent with the photocatalytic HER activity. Notably, the 0.1% Ni_2-Pt_1 has a markedly longer charge carrier lifetime than 0.033% Pt with the same Pt content, which once again points out that the participation of Ni NPs play a positive role in retarding the charge carriers' recombination, and therefore slows down the decay of the signal.

To clarify this hypothesis, the irradiated Ni-Pt co-modified photocatalysts were recovered under argon flow and used for XPS analysis. The presence of low-oxidation forms can be proven by the valence band (VB) XPS spectra (**Figure S10**).[57, 58] After UV-visible light irradiation, there is no significant change in the Ti 2p peaks (**Figure 3a**). The Pt^0 ratio in 0.1% Ni_2-Pt_1/TiO_2 photocatalyst increases significantly after illumination, implying that the electrons generated from TiO_2 are trapped by Pt NPs and resulting in a reduction of Pt^{2+} (**Figure 3c, d**). Meanwhile, the XPS spectra of Ni 2p exhibit a decrease in $Ni^{\sigma+}$ and an increase in Ni^0 content (**Figure 3b, Figure S5**), which may be attributed to the reduction induced by the electrons generated from TiO_2 or its oxides, Ni_xO.

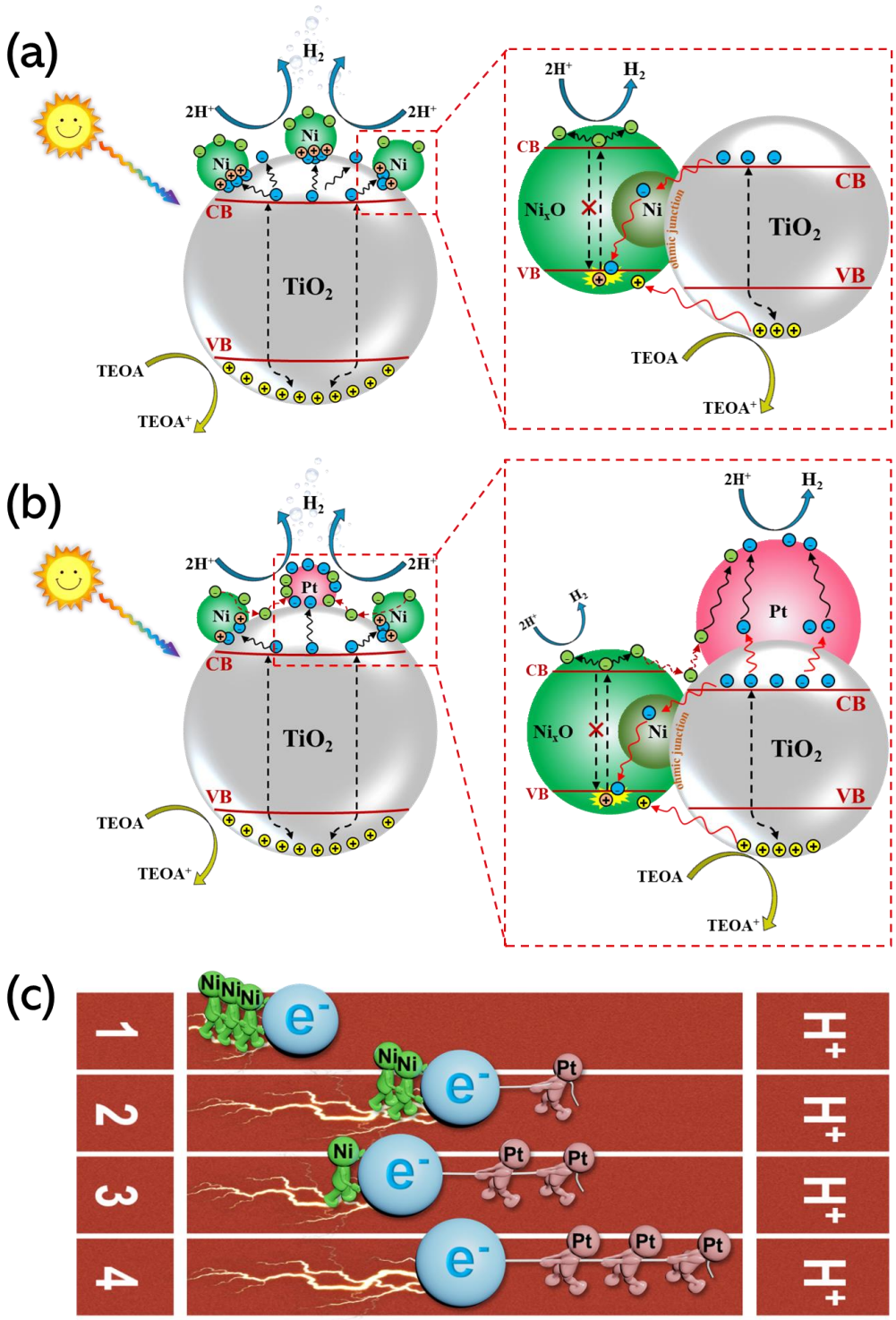

Figure 7. (a, b) Proposed photocatalytic mechanism of monometallic and bimetallic modified TiO_2. (c) Cartoon depictions of different degrees of synergy between Ni and Pt.

Based on the aforementioned characterization results, the photocatalytic mechanisms over monometallic and bimetallic loaded TiO_2 are proposed and illustrated in **Figure 7a, b**. For monometallic Pt modified TiO_2, photogenerated electrons can be excited from the VB of TiO_2 to its CB upon the UV-visible light irradiation, and subsequently migrate to the surface, followed by a rapid transfer and trapping by Pt NPs for supplying the cocatalyst sites. In the circumstance of pure Ni modification, the photons absorption induces excitation of both TiO_2 and Ni_xO, where the electrons from TiO_2 will transfer and combine with the holes of Ni_xO through Ni-TiO_2 Ohmic junction, instead of the formation of Ni_xO-TiO_2 p-n junction.[40] (**Figure 7a**). Consequently, the quantity of photogenerated electrons is approximately identical to that of bare TiO_2, consistent with the

similar I_{max} value observed in TRMC results. Nevertheless, the most striking difference is the electrons provided by Ni_xO, which possess reduced probability of bulk recombination and exhibit a prolonged lifetime and high availability. Compared with monometallic modified TiO_2, the co-modification with Ni and Pt NPs can induce a unique electron transfer pathway, where the Pt NPs serve as electron sinks to attract the photogenerated electrons in their vicinity and Ni NPs act as electron donors (**Figure 7b**). These electrons from Ni NPs can also be capture by Pt NPs, which will downshift the Pt d-band center, and thus further favour the HER.[14] The synergetic effect of Ni and Pt greatly improves the utilization efficiency of photogenerated electrons, endowing Ni-Pt NPs with Pt-like HER activity. Notably, the degree of synergy depends on the Ni/Pt ratio.[11] In alternative words, there is an upper limit to compensating for the loss of active sites by prolonging the electron lifetime (**Figure 7c**). Also, it has been shown in previous studies that Ni NPs can serve as active sites for H$^{\bullet}$ recombination, favouring the formation of H-H bond.[39, 40] According to our optimization, the 0.1%Ni_2-Pt_1/TiO_2 photocatalyst is considered as the most cost-effective candidate with a remarkable stability.

CONCLUSIONS

In summary, we have successfully synthesized ultrasmall Ni and Pt NPs (≈1.9 nm) on the surface of TiO_2 photocatalysts by radiolysis with low metal loading (0.1% in mass). The Ni and Pt NPs are highly dispersed onto the TiO_2 surface, providing a unique electron transfer pathway: (i) the Ni NPs act as electron donors to supply electrons with prolonged lifetime; (ii) the Pt NPs serve as electron acceptors to efficiently trap the electrons from TiO_2 and Ni NPs for offering active sites. This synergy enables Ni-Pt NPs to Pt-like activity in photocatalytic HER, where 0.1%Ni_2-Pt_1/TiO_2 with an apparent quantum yield of 77.5% is found to be the optimal candidate, outperforming about 40-fold higher performance than bare TiO_2-P25. Additionally, this photocatalyst also shows robust stability after five consecutive cycles. This work provides insights into the electron transfer of Ni-Pt co-modified TiO_2 during the photocatalytic HER, and also offers an effective strategy for the rational design of Pt-based cocatalysts, which may help to reduce the usage of Pt and the cost of the photocatalyst, and promote its practical application in solar energy conversion and solar fuels' generation.

ASSOCIATED CONTENT

Supporting Information

The Supporting Information is available free of charge at: https://pubs.acs.org/doi/.

TEM, XPS, electrochemical and photocatalytic experiments (PDF)

AUTHOR INFORMATION

Corresponding Author

Hynd Remita − Institut de Chimie Physique, UMR 8000 CNRS, Université Paris-Saclay, Orsay 91405, France; orcid.org/0000-0003-3698-9327.

Authors

Cong Wang − Institut de Chimie Physique, UMR 8000 CNRS, Université Paris-Saclay, Orsay 91405, France; orcid.org/0000-0002-5071-2562

Christophe Colbeau-Justin − Institut de Chimie Physique, UMR 8000 CNRS, Université Paris-Saclay, Orsay 91405

Diana Dragoe − Institut de Chimie Moléculaire et des Matériaux d'Orsay, UMR 8182 CNRS, Université Paris-Saclay, 91405 Orsay, France

Paul Haghi-Ashtiani − Laboratoire de Mécanique des Sols, Structures et Matériaux, CNRS UMR 8579, CentraleSupélec, Université Paris - Saclay, Gif-sur-Yvette, France

Mohamed Nawfal Ghazzal − Institut de Chimie Physique, UMR 8000 CNRS, Université Paris-Saclay, Orsay 91405, France; orcid.org/0000-0002-2040-995X

Complete contact information is available at: https://pubs.acs.org/10.1021/acsami.XXXXX

Notes

The authors declare no conflict of interest

ACKNOWLEDGMENTS

Cong Wang acknowledges the China Scholarship Council (CSC) for his fellow research position.

REFERENCES

1. Chen, S.; Takata, T.; Domen, K., Particulate photocatalysts for overall water splitting. *Nat. Rev. Mater.* **2017,** *2* (10), 1-17.
2. Wang, Q.; Domen, K., Particulate Photocatalysts for Light-Driven Water Splitting: Mechanisms, Challenges, and Design Strategies. *Chem. Rev.* **2020,** *120* (2), 919-985.
3. Nishiyama, H.; Yamada, T.; Nakabayashi, M.; Maehara, Y.; Yamaguchi, M.; Kuromiya, Y.; Nagatsuma, Y.; Tokudome, H.; Akiyama, S.; Watanabe, T.; Narushima, R.; Okunaka, S.; Shibata, N.; Takata, T.; Hisatomi, T.; Domen, K., Photocatalytic solar hydrogen production from water on a 100 m^2 scale. *Nature* **2021,** *598* (7880), 304-307.
4. Guo, Q.; Zhou, C.; Ma, Z.; Yang, X., Fundamentals of TiO_2 Photocatalysis: Concepts, Mechanisms, and Challenges. *Adv. Mater.* **2019,** *31* (50), 1901997.
5. Wang, C.; Li, J.; Paineau, E.; Laachachi, A.; Colbeau-Justin, C.; Remita, H.; Ghazzal, M. N., A sol–gel biotemplating route with cellulose nanocrystals to design a photocatalyst for improving hydrogen generation. *J. Mater. Chem. A* **2020,** *8* (21), 10779-10786.
6. Schneider, J.; Matsuoka, M.; Takeuchi, M.; Zhang, J.; Horiuchi, Y.; Anpo, M.; Bahnemann, D. W., Understanding TiO_2 photocatalysis: mechanisms and materials. *Chem. Rev.* **2014,** *114* (19), 9919-9986.
7. Rodriguez-Gonzalez, V.; Obregon, S.; Patron-Soberano, O. A.; Terashima, C.; Fujishima, A., An approach to the photocatalytic mechanism in the TiO_2-nanomaterials microorganism interface for the control of infectious processes. *Appl. Catal. B* **2020,** *270*, 118853.
8. Meng, A.; Zhang, L.; Cheng, B.; Yu, J., Dual Cocatalysts in TiO_2 Photocatalysis. *Adv. Mater.* **2019,** *31* (30), 1807660.
9. Liu, Y.; Sun, Z.; Hu, Y. H., Bimetallic cocatalysts for photocatalytic hydrogen production from water. *Chem. Eng. J.* **2021,** *409*, 128250.
10. Greeley, J.; Jaramillo, T. F.; Bonde, J.; Chorkendorff, I. B.; Norskov, J. K., Computational high-throughput screening of electrocatalytic materials for hydrogen evolution. *Nat. Mater.* **2006,** *5* (11), 909-913.

11. Yuan, X.; Dragoe, D.; Beaunier, P.; Uribe, D. B.; Ramos, L.; Méndez-Medrano, M. G.; Remita, H., Polypyrrole nanostructures modified with mono- and bimetallic nanoparticles for photocatalytic H_2 generation. *J. Mater. Chem. A* **2020,** *8* (1), 268-277.
12. Chen, Y.; Ji, S.; Sun, W.; Lei, Y.; Wang, Q.; Li, A.; Chen, W.; Zhou, G.; Zhang, Z.; Wang, Y.; Zheng, L.; Zhang, Q.; Gu, L.; Han, X.; Wang, D.; Li, Y., Engineering the Atomic Interface with Single Platinum Atoms for Enhanced Photocatalytic Hydrogen Production. *Angew. Chem. Int. Ed. Engl.* **2020,** *59* (3), 1295-1301.
13. Bi, L.; Gao, X.; Ma, Z.; Zhang, L.; Wang, D.; Xie, T., Enhanced Separation Efficiency of $PtNi_x$/g-C_3N_4 for Photocatalytic Hydrogen Production. *ChemCatChem* **2017,** *9* (19), 3779-3785.
14. Xinlong Tian; Xiao Zhao; Ya-Qiong Su; Lijuan Wang; Hongming Wang; Dai Dang; Bin Chi; Hongfang Liu; Emiel J.M. Hensen; Xiong Wen (David) Lou; Xia, B. Y., Engineering bunched Pt-Ni alloy nanocages for efficient oxygen reduction in practical fuel cells. *Science* **2019,** *366*, 850–856.
15. Gao, R.; Wang, J.; Huang, Z.-F.; Zhang, R.; Wang, W.; Pan, L.; Zhang, J.; Zhu, W.; Zhang, X.; Shi, C.; Lim, J.; Zou, J.-J., Pt/Fe_2O_3 with Pt–Fe pair sites as a catalyst for oxygen reduction with ultralow Pt loading. *Nat. Energy* **2021,** *6* (6), 614-623.
16. Wang, D.; Li, Y., Effective octadecylamine system for nanocrystal synthesis. *Inorg. Chem.* **2011,** *50* (11), 5196-5202.
17. Lina Chong; Jianguo Wen; Joseph Kubal; Fatih G. Sen; Jianxin Zou; Jeffery Greeley; Maria Chan; Heather Barkholtz; Wenjiang Ding; Liu, D.-J., Ultralow-loading platinum-cobalt fuel cell catalysts derived from imidazolate frameworks. *Science* **2018,** *362* (6420), 1276-1281.
18. Shahvaranfard, F.; Ghigna, P.; Minguzzi, A.; Wierzbicka, E.; Schmuki, P.; Altomare, M., Dewetting of PtCu Nanoalloys on TiO_2 Nanocavities Provides a Synergistic Photocatalytic Enhancement for Efficient H_2 Evolution. *ACS Appl. Mater. Interfaces* **2020,** *12* (34), 38211-38221.
19. Sankar, M.; Dimitratos, N.; Miedziak, P. J.; Wells, P. P.; Kiely, C. J.; Hutchings, G. J., Designing bimetallic catalysts for a green and sustainable future. *Chem. Soc. Rev.* **2012,** *41* (24), 8099-139.
20. Kim, T.-S.; Kim, J.; Song, H. C.; Kim, D.; Jeong, B.; Lee, J.; Shin, J. W.; Ryoo, R.; Park, J. Y., Catalytic Synergy on PtNi Bimetal Catalysts Driven by Interfacial Intermediate Structures. *ACS Catal.* **2020,** *10* (18), 10459-10467.
21. Chen, W.-T.; Chan, A.; Sun-Waterhouse, D.; Moriga, T.; Idriss, H.; Waterhouse, G. I. N., Ni/TiO_2: A promising low-cost photocatalytic system for solar H_2 production from ethanol–water mixtures. *J. Catal.* **2015,** *326*, 43-53.
22. Cao, Z.; Chen, Q.; Zhang, J.; Li, H.; Jiang, Y.; Shen, S.; Fu, G.; Lu, B. A.; Xie, Z.; Zheng, L., Platinum-nickel alloy excavated nano-multipods with hexagonal close-packed structure and superior activity towards hydrogen evolution reaction. *Nat. Commun.* **2017,** *8*, 15131.
23. Xie, Z.; Yan, B.; Lee, J. H.; Wu, Q.; Li, X.; Zhao, B.; Su, D.; Zhang, L.; Chen, J. G., Effects of oxide supports on the CO_2 reforming of ethane over Pt-Ni bimetallic catalysts. *Appl. Catal. B* **2019,** *245*, 376-388.
24. Brian T. Sneed; Allison P. Young; Daniel Jalalpoor; Matthew C. Golden; Shunjia Mao; Ying Jiang; Yong Wang; Tsung, C.-K., Shaped Pd-Ni-Pt Core-Sandwich-Shell Nanoparticles: Influence of Ni Sandwich Layers on Catalytic Electrooxidations. *ACS Nano* **2014,** *8* (7), 7239-7250.
25. Zhao, Z.; Liu, H.; Gao, W.; Xue, W.; Liu, Z.; Huang, J.; Pan, X.; Huang, Y., Surface-Engineered PtNi-O Nanostructure with Record-High Performance for Electrocatalytic Hydrogen Evolution Reaction. *J. Am. Chem. Soc.* **2018,** *140* (29), 9046-9050.
26. C.Stephen Kellner; T.Bell, A., Effects of dispersion on the activity and selectivity of alumina-supported ruthenium catalysts for carbon monoxide hydrogenation. *J. Catal.* **1982,** *75* (2), 251-261.
27. Zhu, J.; Cheng, G.; Xiong, J.; Li, W.; Dou, S., Recent Advances in Cu-Based Cocatalysts toward Solar-to-Hydrogen Evolution: Categories and Roles. *Solar RRL* **2019,** *3* (10), 1900256.
28. Remita, H.; Remita, S., The contribution of radiation chemistry to metal clusters and nanomaterials. *Recent Trends in Radiation Chemistry. World Scientific Publishing Company, London* **2010**, 347-383.
29. Belloni, J.; Mostafavi, M.; Remita, H.; Marignier, J.-L.; Delcourt, a. M.-O., Radiation-induced synthesis of mono- and multi-metallic clusters and nanocolloids. *New J. Chem.* **1998,** *22* (11), 1239-1255.
30. Remita, H.; Lampre, I.; Mostafavi, M.; Balanzat, E.; Bouffard, S., Comparative study of metal clusters induced in aqueous solutions by γ-rays, electron or C6+ ion beam irradiation. *Radiat. Phys. Chem.* **2005,** *72* (5), 575-586.
31. E. Kowalska; H. Remita; C. Colbeau-Justin; J. Hupka; Belloni, J., Modification of Titanium Dioxide with Platinum Ions and Clusters: Application in Photocatalysis. *J. Phys. Chem. C* **2008,** *112* (4), 1124-1131.
32. Abidi, W.; Remita, H., Gold based nanoparticles generated by radiolytic and photolytic methods. *Recent Pat. Eng.* **2010,** *4* (3), 170-188.
33. Remita, H.; Remita, S., Metal clusters and nanomaterials: contribution of radiation chemistry. *Recent trends in radiation chemistry* **2010**, 347-383.
34. Ma, J.; Tan, X.; Zhang, Q.; Wang, Y.; Zhang, J.; Wang, L., Exploring the Size Effect of Pt Nanoparticles on the Photocatalytic Nonoxidative Coupling of Methane. *ACS Catal.* **2021,** *11* (6), 3352-3360.
35. Wang, Z.; Ma, P.; Zheng, K.; Wang, C.; Liu, Y.; Dai, H.; Wang, C.; Hsi, H.-C.; Deng, J., Size effect, mutual inhibition and oxidation mechanism of the catalytic removal of a toluene and acetone mixture over TiO_2 nanosheet-supported Pt nanocatalysts. *Appl. Catal. B* **2020,** *274*, 118963.
36. Yuan, X.; Wang, C.; Dragoe, D.; Beaunier, P.; Colbeau-Justin, C.; Remita, H., Highly Promoted Photocatalytic Hydrogen Generation by Multiple Electron Transfer Pathways. *Appl. Catal. B* **2021,** *281*, 119457.
37. Zeng, B.; Wang, S.; Gao, Y.; Li, G.; Tian, W.; Meeprasert, J.; Li, H.; Xie, H.; Fan, F.; Li, R.; Li, C., Interfacial Modulation with Aluminum Oxide for Efficient Plasmon-Induced Water Oxidation. *Adv. Funct. Mater.* **2020,** *31* (6), 2005688.
38. Wang, K.; Wang, Y.; Geng, S.; Wang, Y.; Song, S., High-Temperature Confinement Synthesis of Supported Pt–Ni Nanoparticles for Efficiently Catalyzing Oxygen Reduction Reaction. *Adv. Funct. Mater.* **2022,** *32* (22), 2113399.
39. Luna, A. L.; Dragoe, D.; Wang, K.; Beaunier, P.; Kowalska, E.; Ohtani, B.; Bahena Uribe, D.; Valenzuela, M. A.; Remita, H.; Colbeau-Justin, C., Photocatalytic Hydrogen Evolution Using Ni–Pd/TiO_2: Correlation of Light Absorption, Charge-Carrier Dynamics, and Quantum Efficiency. *J. Phys. Chem. C* **2017,** *121* (26), 14302-14311.
40. Luna, A. L.; Novoseltceva, E.; Louarn, E.; Beaunier, P.; Kowalska, E.; Ohtani, B.; Valenzuela, M. A.; Remita, H.; Colbeau-Justin, C., Synergetic effect of Ni and Au nanoparticles synthesized on titania particles for efficient photocatalytic hydrogen production. *Appl. Catal. B* **2016,** *191*, 18-28.
41. Baltrusaitis, J.; Mendoza-Sanchez, B.; Fernandez, V.; Veenstra, R.; Dukstiene, N.; Roberts, A.; Fairley, N., Generalized molybdenum oxide surface chemical state XPS determination via informed amorphous sample model. *Appl. Surf. Sci.* **2015,** *326*, 151-161.
42. Sun, S.; Zhang, Y.-C.; Shen, G.; Wang, Y.; Liu, X.; Duan, Z.; Pan, L.; Zhang, X.; Zou, J.-J., Photoinduced composite of Pt decorated $Ni(OH)_2$ as strongly synergetic cocatalyst to boost H_2O activation for photocatalytic overall water splitting. *Appl. Catal. B* **2019,** *243*, 253-261.

43. Fang, S.; Sun, Z.; Hu, Y. H., Insights into the Thermo-Photo Catalytic Production of Hydrogen from Water on a Low-Cost NiO_x-Loaded TiO_2 Catalyst. *ACS Catal.* **2019,** *9* (6), 5047-5056.
44. Meng, A.; Zhang, J.; Xu, D.; Cheng, B.; Yu, J., Enhanced photocatalytic H_2-production activity of anatase TiO_2 nanosheet by selectively depositing dual-cocatalysts on {101} and {001} facets. *Appl. Catal. B* **2016,** *198*, 286-294.
45. Chastain, J.; King Jr, R. C., Handbook of X-ray photoelectron spectroscopy. *Perkin-Elmer Corporation* **1992,** *40*, 221.
46. Wang, Y.; Shang, X.; Shen, J.; Zhang, Z.; Wang, D.; Lin, J.; Wu, J. C. S.; Fu, X.; Wang, X.; Li, C., Direct and indirect Z-scheme heterostructure-coupled photosystem enabling cooperation of CO_2 reduction and H_2O oxidation. *Nat. Commun.* **2020,** *11* (1), 3043.
47. Zou, Y.; Yang, B.; Liu, Y.; Ren, Y.; Ma, J.; Zhou, X.; Cheng, X.; Deng, Y., Controllable Interface-Induced Co-Assembly toward Highly Ordered Mesoporous $Pt@TiO_2/g\text{-}C_3N_4$ Heterojunctions with Enhanced Photocatalytic Performance. *Adv. Funct. Mater.* **2018,** *28* (50), 1806214.
48. Shaban, M.; Poostforooshan, J.; Weber, A. P., Surface-initiated polymerization on unmodified inorganic semiconductor nanoparticles via surfactant-free aerosol-based synthesis toward core–shell nanohybrids with a tunable shell thickness. *J. Mater. Chem. A* **2017,** *5* (35), 18651-18663.
49. Xiao, M.; Zhang, L.; Luo, B.; Lyu, M.; Wang, Z.; Huang, H.; Wang, S.; Du, A.; Wang, L., Molten-Salt-Mediated Synthesis of an Atomic Nickel Co-catalyst on TiO_2 for Improved Photocatalytic H_2 Evolution. *Angew. Chem. Int. Ed. Engl.* **2020,** *59* (18), 7230-7234.
50. Hai, Z.; Kolli, N. E.; Uribe, D. B.; Beaunier, P.; Jose-Yacaman, M.; Vigneron, J.; Etcheberry, A.; Sorgues, S.; Colbeau-Justin, C.; Chen, J.; Remita, H., Modification of TiO_2 by Bimetallic Au-Cu Nanoparticles for Wastewater Treatment. *J. Mater. Chem. A* **2013,** *1* (36), 10829-10835.
51. Schindler K M; M, K., Charge-carrier dynamics in titania powders. *J. Phys. Chem.* **1990,** *94* (21), 8222-8226.
52. C. Colbeau-Justin, M. K., D. Huguenin, Structural influence on charge-carrier lifetimes in TiO_2 powders studied by microwave absorption. *J. Mater. Sci.* **2003,** *38* (11), 2429–2437.
53. Kunst, M.; Beck, G., The study of charge carrier kinetics in semiconductors by microwave conductivity measurements. *J. Appl. Phys.* **1986,** *60* (10), 3558-3566.
54. Kunst, M.; Goubard, F.; Colbeau-Justin, C.; Wünsch, F., Electronic transport in semiconductor nanoparticles for photocatalytic and photovoltaic applications. *Mater. Sci. Eng. C* **2007,** *27* (5-8), 1061-1064.
55. Carina A. Emilio; Marta I. Litter; Marinus Kunst; Michel Bouchard; Colbeau-Justin, C., Phenol Photodegradation on Platinized-TiO_2 Photocatalysts Related to Charge-Carrier Dynamics. *Langmuir* **2006,** *22* (8), 3606-3613.
56. Ran, J.; Zhang, J.; Yu, J.; Jaroniec, M.; Qiao, S. Z., Earth-abundant cocatalysts for semiconductor-based photocatalytic water splitting. *Chem. Soc. Rev.* **2014,** *43* (22), 7787-7812.
57. Cai, J.; Wu, M.; Wang, Y.; Zhang, H.; Meng, M.; Tian, Y.; Li, X.; Zhang, J.; Zheng, L.; Gong, J., Synergetic Enhancement of Light Harvesting and Charge Separation over Surface-Disorder-Engineered TiO_2 Photonic Crystals. *Chem* **2017,** *2* (6), 877-892.
58. El Jamal, G.; Gouder, T.; Eloirdi, R.; Jonsson, M., X-Ray and ultraviolet photoelectron spectroscopy studies of Uranium(IV), (V) and(VI) exposed to H_2O-plasma under UHV conditions. *Dalton Trans.* **2021,** *50* (2), 729-738.

Table of Contents